JOURNAL OF MATERIALS SCIENCE 11 (1976) 1310–1319

Fracture surface analysis of ceramics

J. J. MECHOLSKY JUN, S. W. FREIMAM, R. W. RICE
Naval Research Laboratory, Washington, D.C., USA

Flaw size, c, fracture mirror boundaries, r, fracture stress, σ, and critical fracture energy were measured for glasses, glass ceramics, and single and polycrystalline ceramics. The relationship $\sigma r^{1/2}$ = constant was verified for all these materials. The mirror constants, A, in these materials were shown to be directly proportional to the average critical stress intensity factor for crack propagation, K_{IC}. Based on the $A - K_{IC}$ relationship, the outer mirror to flaw size ratio is shown to scatter about a value of 13:1. Thus, the mirror constants were used to predict critical flaw sizes in these materials. The observed flaw sizes in most cases correlated well with those calculated. The cases in which poorer correlation was obtained are those in which flaw sizes were smaller than the grain size, flaws were pores or surrounded by porous regions, or where severe microcracking existed. It is shown that the elastic modulus is proportional to the mirror constant and probably to the critical fracture energy, but that the latter is highly dependent on local microstructure. The smaller inner to outer mirror ratios for polycrystalline ceramics over glasses is attributed to the difference in available paths for crack propagation.

1. Introduction

One of the important aspects of fracture mechanics as applied to ceramics is its usefulness in predicting critical flaw sizes which can be correlated with processing or machining parameters. The general expression used to calculate critical flaw size, c, is [1]:

$$c = \frac{Y^2}{2}\frac{(2E\gamma_c)}{\sigma^2} = \frac{Y^2}{2}\frac{K_{IC}^2}{\sigma^2}, \quad (1)$$

where σ is the fracture stress, E the elastic modulus, γ_c the critical fracture energy, and Y a constant which depends on the flaw geometry. In part because of the difficulty in distinguishing the critical flaws on many polycrystalline fracture surfaces, few correlations between calculated and observed flaw sizes have been reported [2].

One solution to this problem involves the use of fracture mirror sizes to predict both failure stresses and flaw sizes. The relation between mirror size and fracture stress, σ, for both glasses and ceramics is given by:

$$\sigma = Ar^{-1/2} \quad (2)$$

where A is a materials' constant and r is the mirror radius, i.e., the distance along the fracture surface from the point of fracture initiation to either the mirror–mist or mist–hackle boundary. It has been shown that for most glasses, analysis of fracture mirrors can be used to predict both critical fracture energies and flaw sizes. The outer mirror (hackle) and inner mirror (mist) to flaw size ratios were shown to be 13/1 and 10/1, respectively, for most silicate glasses [1].

The purpose of the present study was to determine whether such a relationship between mirror and flaw sizes also held for polycrystalline ceramics of various compositions and microstructures as well as single crystals, and if so, to establish these relations. Since this entails independent measurements of σ, c, γ, and E, it allows a determination of the accuracy with which fracture mechanics apply to the prediction of failure of polycrystalline ceramics. In addition, it will be shown that fracture surface features in polycrystalline ceramics can help provide other insights into the fracture process.

2. Experimental procedure

Fracture energy measurements were performed using a modification of the double-cantilever beam technique [3] using specimens ≈ 50 mm

× 13 mm × 2 mm containing a centre groove to guide the crack. In most instances, a notch was sawed in one end of the specimen, but no sharp crack was introduced. No significant difference in γ_c was observed between those specimens containing a crack and those in which the crack started from the notch. Critical fracture energies were determined by loading these specimens at a rate of 2 mm min^{-1}* until the crack propagated rapidly. γ_c was then calculated from the expression

$$\gamma_c = \frac{P^2L^2}{2EIt} \quad (3)$$

where E is elastic modulus (for the single crystals, the E in the direction of crack propagation), I is the moment of inertia of the specimen about its longitudinal axis, t is the specimen thickness at the groove, P is the load on one arm, and L is the length of the moment arm. All measurements were made in air (~ 40% r.h.) at room temperature.

The halves of the fracture energy specimens

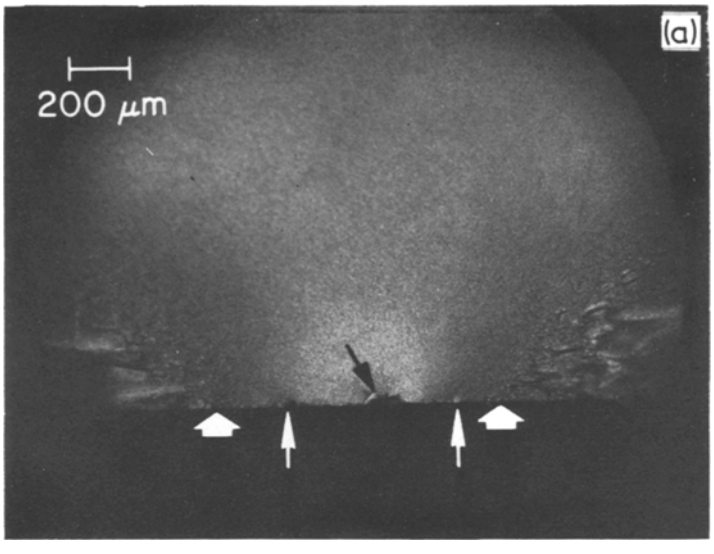

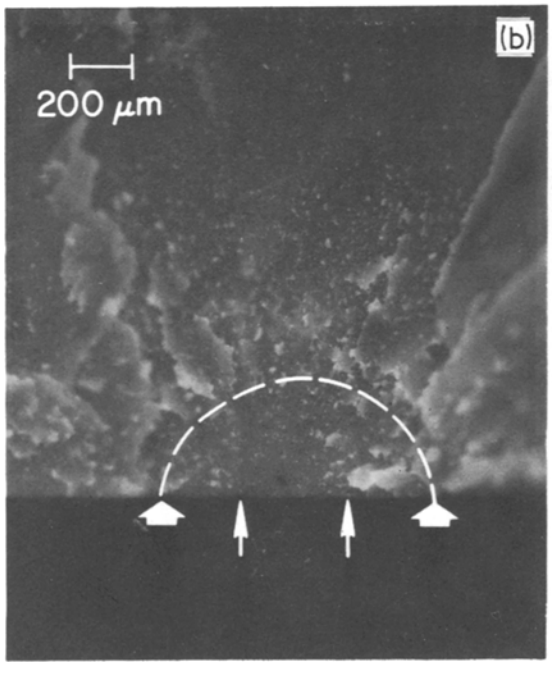

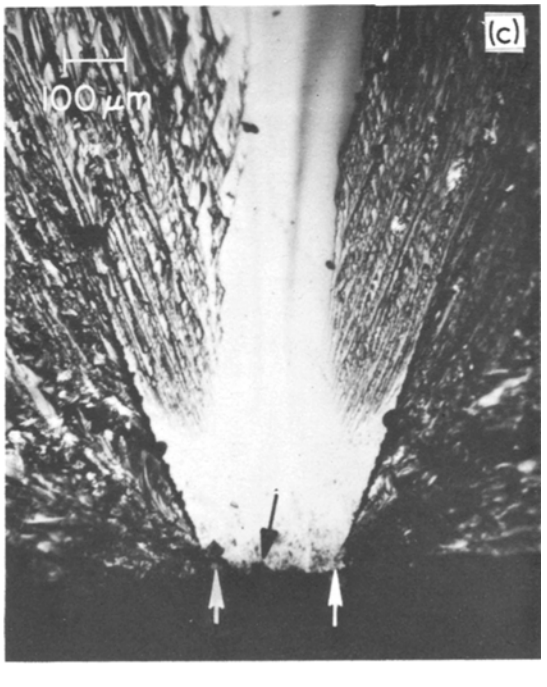

Figure 1 Optical fractographs of (a) $3BaO \cdot 5SiO_2$ glass-ceramic; (b) hot-pressed Si_3N_4; and (c) single crystal ammonium diphosphate (ADP). Broad arrows indicate outer mirror demarcations; thin arrows in a and b indicate inner mirror boundaries; thin arrows in (c) may be outer mirror boundary with no inner mirror (mist) boundary present. Black arrows indicate machined flaws which acted as the source of failure. The failure origin in (b) is the black dot approximately in the centre of the broad arrows. The dashed line is just inside the outline of the outer mirror.

*Instron test machine.

were used as flexure test bars; many other test bars were also prepared. As-ground bars ≈ 5 mm x 2.5 mm in cross-section and having a span length of 12.7 mm were loaded in three-point bending† at a rate of 1.27 mm min^{-1}. Fracture surfaces were examined optically and the size of the features measured using a filar eyepiece. Mirror dimensions were always taken along the tensile surface for reasons discussed elsewhere [1]. For ease of analysis, only approximately semi-circular flaws were considered in this study, but other work [4] has shown that semi-elliptical flaws are also valid if the flaw geometry is considered, and provided the minor axis of the flaw is taken as its size.

Elastic modulus data was obtained from the literature.

3. Results and discussion

3.1. Fracture surface topography

Micrographs of representative fracture surfaces of several ceramics, showing the area of fracture initiation, are presented in Fig. 1. The beginning of hackle is clearly evident on these micrographs, as it was on most of the other ceramics examined, and closely resembles that obversed on glasses. While there was some evidence of mist formation, the fracture surface appearance in polycrystalline ceramics differs somewhat from that in glasses. While there is some evidence of mist formation, almost always discernible, in polycrystalline ceramics this feature is more difficult to define, especially in large grain or highly porous materials. In large grain ceramics, many of the cleavage steps left from transgranular failure focus onto the

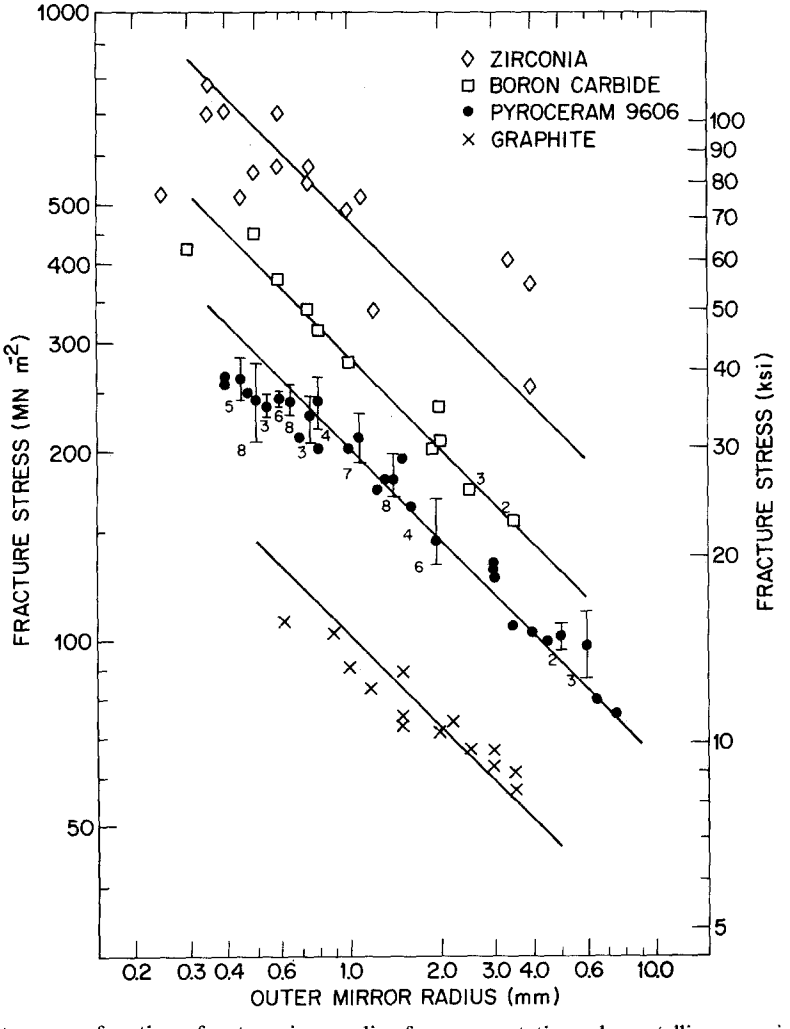

Figure 2 Fracture stress as a function of outer mirror radius for representative polycrystalline ceramics. Solid lines are least squares fit of slope -0.5. 10^3 psi = 1 ksi.

†Ametek test machine.

fracture origin, thus making identification of the source of failure easier [5]. Cleavage steps as well as hackle markings also appear on the fracture surfaces of single crystals depending on the orientation of crack propagation. However, in single crystals the occurrence of mist and hackle depends on the fracture plane and the direction of propagation on this plane. In most ceramics there is an identifiable region surrounding the failure origin that reflects light better than regions further from the origin, and is usually bounded by small flake-like particles (mist).

Logarithmic plots of flexural strength versus the outer mirror radius are presented in Fig. 2 for representative materials: Pyroceram 9606, Poco Graphite, B_4C, and ZrO_2 (Zircar). The curves are the best fit straight lines of slope -0.5. The use of this slope is based on the assumption that Equation 2 is valid for ceramics. In many cases the best linear least squares fit had a slope of ~ -0.5. The data for glasses [1] were given in a previous paper. Strength–mirror size curves for ADP [6], hot-pressed Al_2O_3 [7], sapphire [8], Si_3N_4 [9], and AlSiMag 614 [9] are also given in the literature; however, more extensive data on both inner and outer mirror radii for these materials were also taken in the present study. Both inner and outer mirror constants obtained in this work are presented in Table I. The flaw sizes at the source of failure were measured for all materials, and are also presented in Table I.

3.2. Fracture mechanics analysis

In order to compare flaw sizes calculated using a fracture mechanics approach with those observed at the failure origin for these wide varieties of materials it was necessary to account for the fact that they may have widely differing flaw size distributions. This, of course, is the difficulty in comparing literature data of different investigators, since variations in processing and machining often give different flaw populations, and different test parameters may further shift the sizes of flaws causing failure. This problem can be solved by normalizing the strength of these materials at a given fracture mirror size.

$$A = \sigma r^{1/2} = \frac{Y}{\sqrt{2}} \frac{K_{IC}}{(c/r)^{1/2}}. \quad (4)$$

Equation 4* relates fracture surface analysis (Equation 2) to fracture mechanics (Equation 1).

*For $r = c$ this reduces to Equation 1.

Notice that at an outer mirror radius of 1 mm the mirror constant may be considered a normalized stress. Equation 4 is plotted in Fig. 3. Almost all of the data (Fig. 3) fall within a band centred on a mirror to flaw size ratio of 13:1. There is no evidence to suggest that points falling either above or below the trend line represent failure of a particular type; e.g. machining flaws, pores, large grains, etc. This trend implies that the ratio of outer mirror size to flaw size is a constant in glasses and ceramics, independent of crystal structure, composition or microstructure.

The data in Fig. 3 would tend to suggest that Equation 1 is valid for a wide range of ceramics and that if a mirror size can be measured on a fracture surface, then provided γ_c and E are known, an estimate of the flaw size can be obtained as illustrated in Table I. However, the validity of this approach will be shown to depend on the ratio of flaw to grain sizes. Each of the flaw sizes in Table I was calculated from Equation 4 using the mirror constants and average values of E and γ_c for each material, at a mirror size of 1 mm and assuming $Y = 1.12$, corresponding to a penny shaped (semi-circular) flaw. The generally excellent agreement with flaw sizes actually observed on the fracture surface of specimens having 1 mm mirrors confirms the validity of this procedure (Table I). The greatest differences between calculated and observed values occur in $BaTiO_3$, PZT and ZnSe and the two $Li_2O{\cdot}2SiO_2$ glass-ceramics. In PZT [10] and $BaTiO_3$, [11] interior pores rather than surface flaws generally are the source of failure. The predicted values of flaw size for these materials support the concept that the flaw consists of the pore plus one to two surrounding grains [2]. The large values of the calculated flaw sizes in ZnSe illustrates the point, discussed elsewhere [12], that a value of γ_c approaching that of the single crystal is appropriate for materials in which flaws are contained within one or two grains. Because of the large size of the crack compared to the microstructure, the stress intensity at the mirror boundary, as represented by the mirror constant, A, is a measure of the average fracture toughness of the material. It should, therefore, not be surprising that this value cannot be used to predict failure conditions where the local properties of the material at the crack tip differ from the average, e.g. as in the important and frequent case of bodies having grains

TABLE I

Material	Source	Grain size (μm)	Elastic modulus ($MN\,m^{-2} \times 10^4$)	Fracture energy ($J\,m^{-2}$)	Mirror constants[a] ($MN\,m^{-3/2}$)		Observed[b] flaw size (μm)		Predicted[c] flaw size (μm)
		G	E	γ	A_i	A_o	a	b	c
Silicate glasses[†]	Corning Glass		6.4	3.7	1.9	2.1	80	80	67
Glassy carbon	Beckwith Inc.		2.5	8.5	1.2	1.7			92
ADP	NRL	S.C.	0.9	2[d]		0.5	270	600	90
Al_2O_3 (sapphire)	Union Carbide	S.C.	34	7[e]		6.1[§]	50	50	80
$MgAl_2O_4$	Union Carbide	S.C.	24	1[f]		2.6	35	30	44
MgO	Norton Co.	S.C.	28	3[f]		5			42
H.P.Al_2O_3 (99 +)	NRL	1–10	39	20	5.2	12	45	60	68
Alsimag 614	American Lava	2–40	30	20		13.1	24*		44
β–Al_2O_3	NRL	5–20	21	13		~6.5	80	40	82
$BaTiO_2$	Clevite Corp.	5	12	5		5.0	27	36	30
$BaTiO_2$ (LiF–MgO)	NRL	1–20	12	6		5.4	40*	40*	46
B_4C	Norton Co.	20	45	15	4.8	9.27	75	75	98
Graphite	POCO Graphite, Inc.	8	1.2	85		3.32	110	110	116
$MgAl_2O_4$	NRL	<10	24	6	4.0	7.8	25	25	30
MgF_2	Kodak	<1	11	4	1.8	3.1	60	60	57
MgO	NRL	2–20	28	12		9.6	65		46
Mullite	Lehigh Univ.		22.2	11		6.1	60	50	82
PZT	Channel Ind.	5	8	4	1.70	3.7	38	30	29
SiC (KT)	Norton Co.	10–100	39	19		10.7	115	115	82
Si_3N_4 (HS–130)	Norton Co.	~1	31	45		18.1			53
Si_3N_4 (B)	Beckwith Inc.	~1	28	30		12	60	55	73
$SrZrO_3$	Alfred Univ.	5–10	28	6	4.4	6.0	75	60	58
ZnSe	Raytheon	20–30	6.9	4		1.7[‡]	25	40	115
ZrO_2 (Zircar)	Alfred Univ.	0.4	28	70		15.2	200	200	106
ZrO_2 (Zyttrite)	Union Carbide AFML	10	26	13		7.4	90	90	77
$3BaO \cdot SiO_2$	NRL	3–5	9	17	3.9	6.0	70	68	53
Cervit 126	Owens Illinois	<1	9.2	17	4.7	5.9	50	60	56
$Li_2O \cdot 2SiO_2$	NRL	10–20	9	95	3.8	5.4	80	75	367
$Li_2O \cdot 2SiO_2$	NRL	10–20	9	34	3.3	4.5	65	75	190
Pyroceram 9606	Corning Glass	<1	12	25	3.6	6.5	100	100	89

[a] $\sigma r_i^{1/2} = A_i$; $\sigma r_o^{1/2} = A_o$ (selected at $r = 1$ mm)
[b] A = depth; B = half-width; selected at $r = 1.0$ mm.
[c] $c = (Y^2 E\gamma/\sigma^2)$; $\sigma^2 = (A_o^2/10^{-3})$ for $r = 1.0$ mm; c compares with a or b, whichever is smaller.
[d] $\{1\,1\,0\}$ plane
[e] $\{1\,0\,\bar{1}\,0\}$ plane
[f] $\{1\,0\,0\}$ plane
[†] e.g. Borosilicate glass (Corning 7740)
[‡] Crack branching radius
* Pore radius
[§] Average for four different crystal planes.

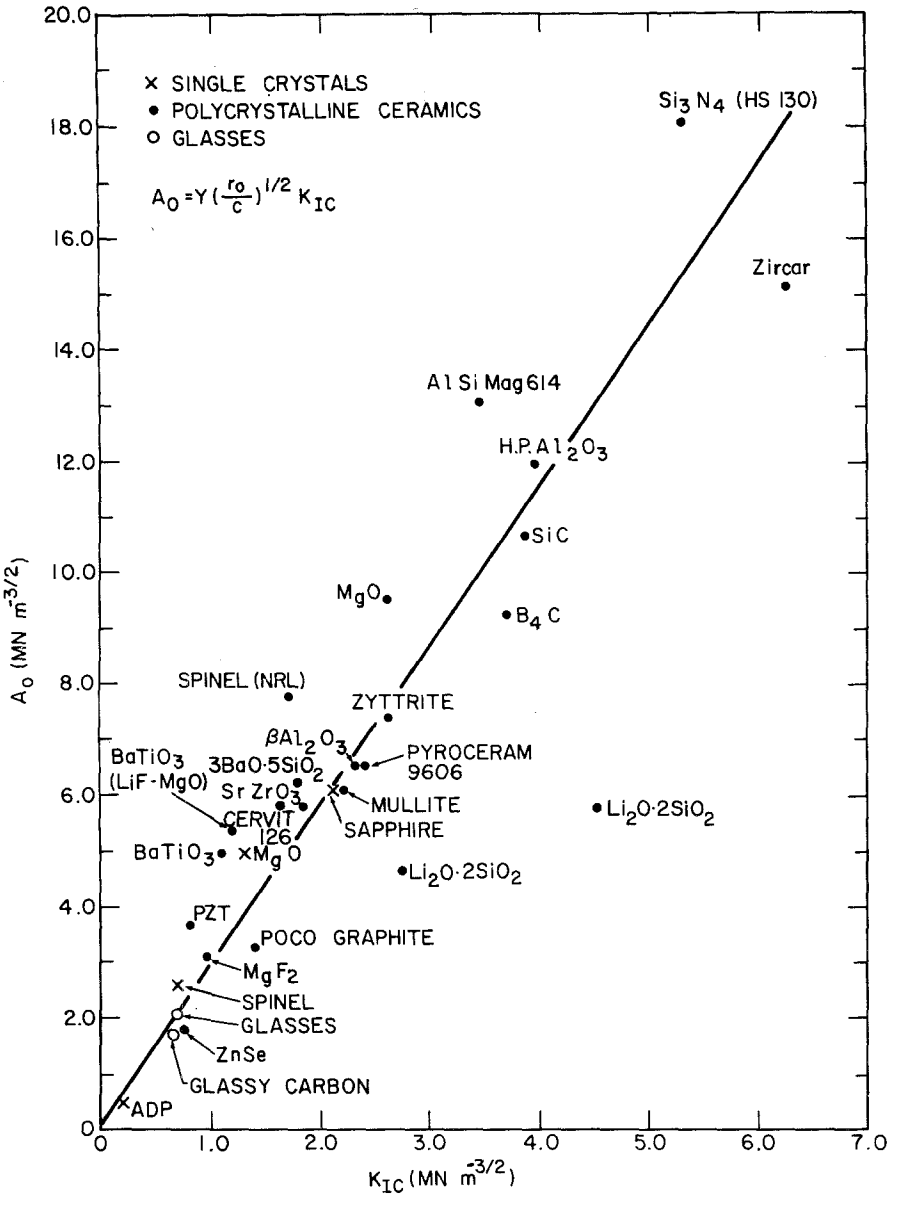

Figure 3 (Outer) mirror constant, A_o, as a function of the critical stress intensity factor, K_{IC} for ceramic materials.

sufficiently large to contain failure initiating flaws. The large value of the predicted flaw size in the $Li_2O \cdot SiO_2$ glass-ceramics compared to that observed is attributed to extensive microcracking, adding to the large values of γ_c.

Because it is related to the average resistance to crack propagation, one might expect that A should be a function of the bond strength of a material and, therefore, of its elastic modulus. The expected relationship of A to E is shown to hold generally for a wide variety of ceramics in Fig. 4. In general, the data obtained in this study agree well with those of Kirchner *et al.* [13]. No reason for the difference in the positions of HS130 Si_3N_4 in the plot is known. The fact that the single crystal points (spinel, MgO, sapphire) fall well below the curve is good evidence for the tendency of grain misorientations in polycrystals to increase fracture toughness. B_4C also falls below the curve because it contains grains sufficiently large to contain flaws within about 1 grain. There also appears to be a series of materials that fall above the general trend with the deviation increasing with increasing E.

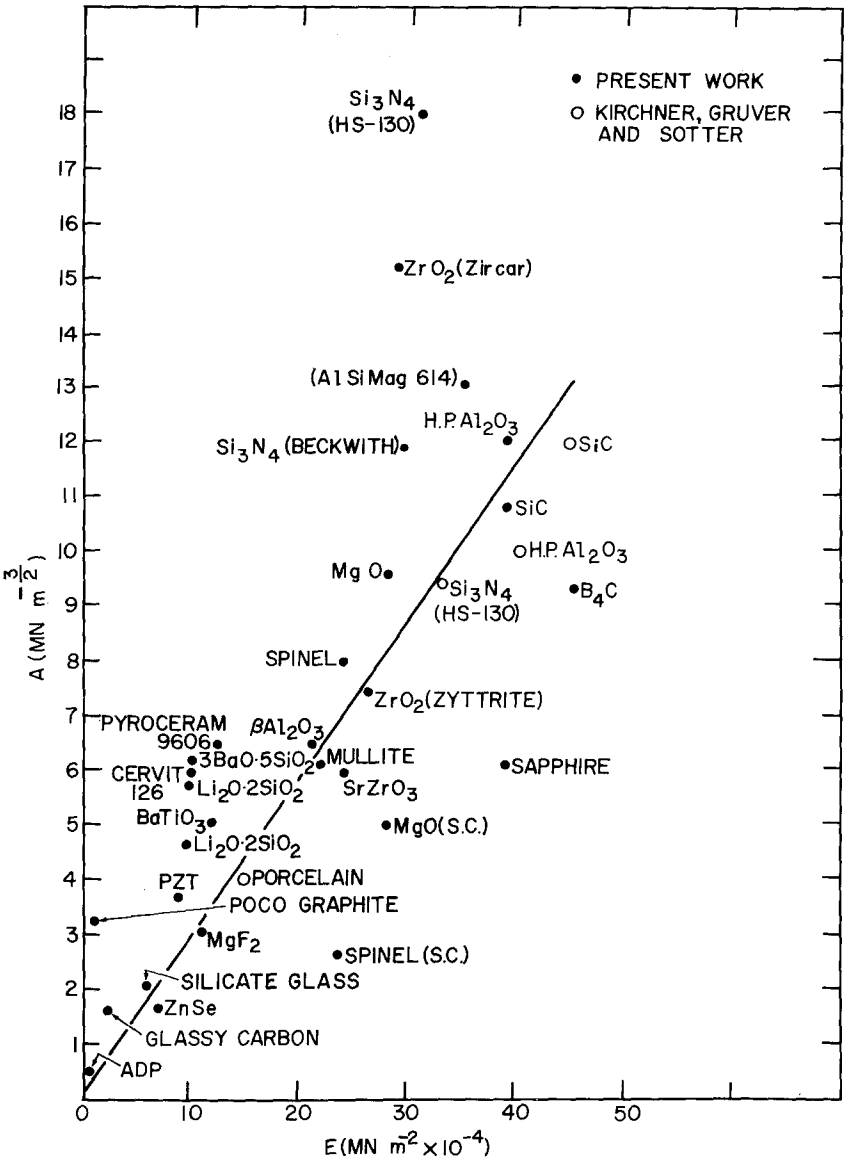

Figure 4 (Outer) mirror constant, A_o, as a function of elastic (Young's) modulus, E, for ceramics. Generally single crystals fall below the indicated trend (solid line) and materials that microcrack fall above. The open circles are from [7] and [13].

If A is proportional to E as indicated in Fig. 4, and A is proportional to K_{IC} as shown in Fig. 3 then $\gamma_c = [K_{IC}^2/2E]$ should be proportional to E. The plot of γ_c as a function of E (Fig. 5) generally shows this trend (cross-hatched area in Fig. 5) but the deviations from the trend appear even greater than those in Fig. 4. As expected, the single crystals fall at low values of γ_c. Of greater interest are those materials falling well above the general trend. These include all the glass-ceramics, graphite and glassy carbon, Si_3N_4's and ZrO_2 (Zircar). It is suggested that the fracture energies of these materials are high, based on that expected from their elastic modulus, because of the presence of microcracking at the tip of a primary crack, which would be an energy absorbing process in the materials. Microcracking in POCO graphite [14] and the $Li_2O \cdot 2SiO_2$ glass-ceramics [15–16] is well estabilshed. The large fracture toughness of a partially stabilized ZrO_2 has been shown to be due to a microcracked zone at the crack tip [17]. The anisotropic crystals in many glass-ceramics plus the existence of a lower strength, glassy grain-boundary phase would increase the likelihood of

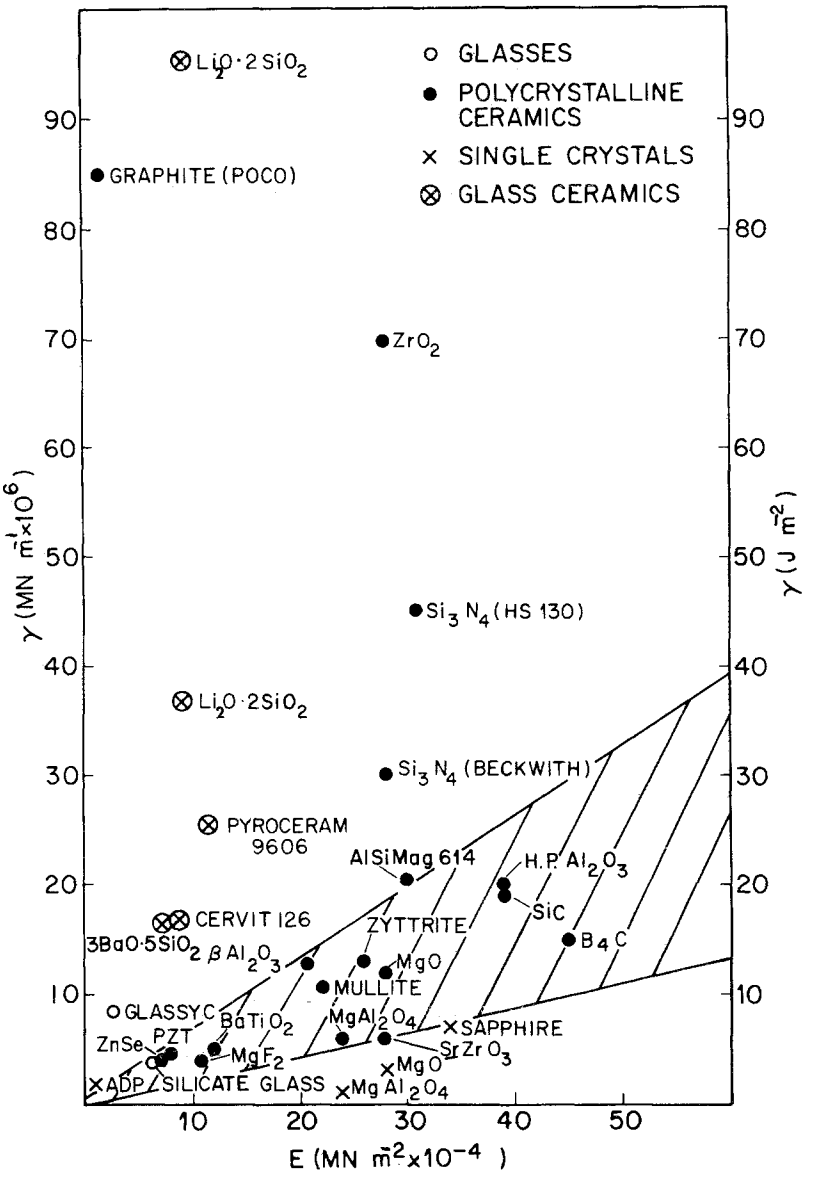

Figure 5 Critical fracture energy, γ_c, as a function of the elastic modulus, E. Single crystals generally fall below the indicated trend (cross-hatched area) and materials that microcrack fall above the trend.

microcracking. Similar factors could also account for microcracking in Si_3N_4 since it is an anisotropic material whose grain boundaries are of a different composition than the grains*.

Thus, Figs. 3, 4 and 5 demonstrate that E, A, and K_{IC}† are average properties of materials and reflect the average differences of glasses, single crystal, and polycrystalline ceramics, whereas the critical fracture energy is a local property of the material at the crack tip and can be heavily influenced by local microstructural fracture processes.

3.3. Crack propagation

As seen in Table II, there can be a significant difference between both the outer and inner mirror to flaw size ratio in polycrystalline ceramics and that observed for silicate glasses. While the former is the same for polycrystalline ceramics and glasses, the latter is significantly smaller, e.g.

*Note added in proof: Microscopic crack branching in Si_3N_4 has recently been observed at NRL.

†Actually K_{IC} reflects both an average and local property, but evidently (Fig. 3) the average property effect is greater.

TABLE II

Material	Mirror to flaw size ratio		Inner mirror to outer mirror ratio
	Inner	Outer	
Silicate glasses	10	13	0.77
As_2S_3 glass	8	13	0.63
Glassy carbon	5	8	0.63
$BaO–SiO_2$ glass-ceramic	7	17	0.42
MgF_2	7	17	0.41
Pyroceram	3	10	0.30
B_4C	4	13	0.31
Spinel	10	40	0.25
PZT	7	33	0.21
Al_2O_3	4	22	0.18

6:1 compared to 10:1. The differences in the flaw to mirror size ratios and inner mirror to outer mirror size ratios between glasses, single crystals and polycrystalline ceramics may be explained by the difference in the process of crack initiation in the materials.

When a flaw begins to propagate as a sharp crack, its velocity of propagation increases with increasing crack length until it nears the terminal velocity for that material, $\approx 0.6\ V_s$, where V_s is the shear wave velocity. Since the energy associated with the lengthening crack plus its kinetic energy can no longer be used to increase its velocity, other processes commence. The first is the nucleation in the vicinity of the tip of the primary crack of the microcracks (mist) which are energetically unable to propagate over larger distances. In glasses the energy needed to initiate or propagate a secondary crack is isotropic so it is expected that the formation of mist would occur at an energy† near that required to form hackle. In single crystals, the energy to initiate fracture is related to the crystallographic direction, the propagation is then related to the elastic properties on the plane of propagation, i.e. the energy required for formation of mist and hackle depends on the plane and direction of crack propagation. In polycrystalline ceramics, however, secondary cracks can be nucleated on cleavage planes within grains at energies at or near those of single crystals, and hence much less than that required to propagate the primary crack through the polycrystalline microstructure. For example, in alumina the fracture energy on the easiest cleavage plane is $\approx 6\,J\,m^{-2}$ compared to 20 to $30\,J\,m^{-2}$ for the polycrystalline body. Because of the lower energy requirements for formation of these cleavage cracks, they would be expected to occur at shorter crack lengths than if they required the same energy as general crack propagation. Thus, the inner mirror size should be smaller than in glasses where all fracture energies are equal. For these cleavage cracks to extend to form hackle, which require higher energies because of their multi-grain extent, means that more energy must be supplied to the fracture process because of that used in mist formation. In polycrystalline ceramics this energy (either potential or kinematic) comes from the greater extension of cracks away from the mist boundary leading to greater ratios of outer to inner radii.

† This is proportional to the mirror–flaw size ratio.

4. Conclusions

(1) The mirror constants for glasses, single and polycrystalline ceramics is directly proportional to the "average" critical stress intensity factor for crack propagation, K_{IC}.

(2) The outer mirror to flaw size ratio for single crystals, polycrystalline ceramics, and glasses scatters about a value of 13:1. However, the inner mirror to flaw size ratio is generally less (6:1) for crystalline ceramics than glasses (10:1) and the ratio of inner to outer mirror is significantly smaller.

(3) The critical fracture energy appears to be a function of elastic modulus for both single crystals and polycrystalline ceramics. However, this relationship is highly dependent on the local processes like microcracking.

(4) The mirror constants can be used to predict flaw sizes or fracture energy in single crystals and glasses, as well as polycrystalline ceramics provided the flaw sizes in the latter are larger than the grain size.

Acknowledgements

The authors thank J. Breen for machining the ceramics. We gratefully acknowledge Dr W. J. McDonough for making several of the materials. We especially thank Drs P. F. Becher and R. C. Pohanka for providing the strength–mirror size data on sapphire and ADP, respectively, and Dr Pohanka for the micrograph. This study was performed on ONR funding (NRL No. 63C05-28).

References

1. J. J. MECHOLSKY, R. W. RICE and S. W. FREIMAN, *J. Amer. Ceram. Soc.* **57** (1974) 440.

2. R. W. RICE, *Fracture Mech. Ceram.* **1** (1974) 323.
3. S. W. FREIMAN, D. R. MULVILLE and P. W. MAST, *J. Mater. Sci.* **8** (1973) 1527.
4. J. J. MECHOLSKY, S. W. FREIMAN and R. W. RICE, Presented at Fall Meeting of the Glass Division, Am. Ceram. Soc. (1975).
5. R. W. RICE, *Mats. Sci. Res.* **7** (1973) 439.
6. R. C. POHANKA, P. L. SMITH and J. PASTERNAK, Report of NRL Progress (January 1975) p. 21.
7. H. P. KIRCHNER and R. M. GRUVER, *Phil. Mag.* **27** (1973) 1433.
8. P. F. BECHER (NRL), private communication.
9. H. P. KIRCHNER and R. M. GRUVER, *Fracture Mech. Ceram.* **1** (1974) 309.
10. B. K. MOLNAR and R. W. RICE, *Bull. Amer. Ceram. Soc.* **52** (1973) 505.
11. R. C. POHANKA, R. W. RICE and B. F. WALKER, *J. Amer. Ceram. Soc.* **59** (1976) 71.
12. S. W. FREIMAN, J. J. MECHOLSKY, R. W. RICE and J. C. WURST, *ibid* **58** (1975) 406.
13. H. P. KIRCHNER, R. M. GRUVER and W. A. SOTTER, Tech. Rpt. No. 2, Contract No. N00014-74-C-0241 (November 1974).
14. R. A. MEYER, J. ZIMMER and M. C. ALMON, Aerospace Rpt. No. ATR-74(7408)-2 (March 1974).
15. M. SAHOO, A. S. RAO and J. S. NADEAU, Report, Centre for Materials Research, University of British Columbia (1972).
16. S. W. FREIMAN and L. L. HENCH, *J. Amer. Ceram. Soc.* **55** (1972) 86.
17. D. J. GREEN, P. S. NICHOLSON and J. D. EMBURY, *ibid* **56** (1973) 619.

Received 28 October and accepted 25 November 1975.